Zhang, Wen Qi; Afshar Vahid, Shahraam; Monro, Tanya Mary.
A genetic algorithm based approach to fiber design for high coherence and large bandwidth supercontinuum generation, *Optics Express*, 2009; 17(21):19311-19327.

# A genetic algorithm based approach to fiber design for high coherence and large bandwidth supercontinuum generation

**Wen Qi Zhang, Shahraam Afshar V. and Tanya M. Monro**

*Centre of Expertise in Photonics, Institute for Photonics & Advanced Sensing, University of Adelaide, Adelaide, SA 5005, Australia*

wen.zhang@adelaide.edu.au, shahraam.afshar@adelaide.edu.au, tanya.monro@adelaide.edu.au

**Abstract:** We present a new approach to the design of optical microstructured fibers that have group velocity dispersion (GVD) and effective nonlinear coefficient ($\gamma$) tailored for supercontinuum (SC) generation. This hybrid approach combines a genetic algorithm (GA) with pulse propagation modeling, but without include it into the GA loop, to allow the efficient design of fibers that are capable of generating highly coherent and large bandwidth SC in the mid-infrared (Mid-IR) spectrum. To the best of our knowledge, this is the first use of a GA to design fiber for SC generation. We investigate the robustness of these fiber designs to variation in the fiber's structural parameters. The optimized fiber structure based on a type of tellurite glass ($70TeO_2 - 10Na_2O - 20ZnF_2$) is predicted to have near-zero group velocity dispersion ($< \pm 2ps/nm/km$) from 2 to 3 $\mu m$, and a effective nonlinear coefficient of $\gamma \approx 174W^{-1}km^{-1}$ at 2 $\mu m$. The SC output of this fiber shows a significant bandwidth and coherence increase compare to a fiber with a single zero group velocity dispersion wavelength at 2 $\mu m$.



**OCIS codes:** (030.1640) Coherence; (060.2280) Fiber design and fabrication; (060.4005) Microstructured fibers; (060.5295) Photonic crystal fibers; (260.2030) Dispersion; (260.3060) Infrared; (320.6629) Supercontinuum generation.

## References and links

1. R. R. Alfano and S. L. Shapiro, "Emission in the region 4000 to 7000 Å via Four-Photon coupling in glass," Phys. Rev. Lett. **24**, 584 (1970).
2. R. R. Alfano and S. L. Shapiro, "Observation of Self-Phase modulation and Small-Scale filaments in crystals and glasses," Phys. Rev. Lett. **24**, 592 (1970).
3. S. Kaasalainen, T. Lindroos, and J. Hyyppa, "Toward hyperspectral lidar: Measurement of spectral backscatter intensity with a supercontinuum laser source," IEEE Geosci. Remote Sens. Lett. **4**, 211–215 (2007).
4. C. Colley, J. Hebden, D. Delpy, A. Cambrey, R. Brown, E. Zibik, W. Ng, L. Wilson, and J. Cockburn, "Mid-infrared optical coherence tomography," Rev. Sci. Instrum. **78** (2007).
5. J. Hult, R. S. Watt, and C. F. Kaminski, "High bandwidth absorption spectroscopy with a dispersed supercontinuum source," Opt. Express **15**, 11385–11395 (2007).
6. K. Shi, P. Li, and Z. Liu, "Broadband coherent anti-Stokes raman scattering spectroscopy in supercontinuum optical trap," Appl. Phys. Lett. **90** (2007).
7. H. Kano and H. o Hamaguchi, "Coherent raman imaging of human living cells using a supercontinuum light source," Jpn. J. Appl. Phys. 1 **46**, 6875–6877 (2007).
8. D. Pestov, X. Wang, G. Ariunbold, R. Murawski, V. Sautenkov, A. Dogariu, A. Sokolov, and M. Scully, "Single-shot detection of bacterial endospores via coherent raman spectroscopy," P. Natl. Acad. Sci. USA **105**, 422–427 (2008).

9. T. M. Monro and H. Ebendorff-Heidepriem, "Progress in microstructured optical fibers," Annu. Rev. Mater. Res. **36**, 467–495 (2006).
10. W. Zhang, S. V, H. Ebendorff-Heidepriem, and T. Monro, "Record nonlinearity in optical fibre," Electron. Lett. **44**, 1453–1455 (2008).
11. C. Xia, M. Kumar, O. R. Kulkarni, M. N. Islam, F. L. Terry, and M. J. Freeman, "Mid-infrared supercontinuum generation to 4.5 mu m in ZBLAN fluoride fibers by nanosecond diode pumping," Opt. Lett. **31**, 2553–2555 (2006).
12. J. H. V. Price, T. M. Monro, H. Ebendorff-Heidepriem, F. Poletti, P. Horak, V. Finazzi, J. Y. Y. Leong, P. Petropoulos, J. C. Flanagan, G. Brambilla, M. Feng, and D. J. Richardson, "Mid-IR supercontinuum generation from nonsilica microstructured optical fibers," IEEE J. Sel. Topics Quantum Electron. **13**, 738–749 (2007).
13. P. Domachuk, N. A. Wolchover, M. Cronin-Golomb, A. Wang, A. K. George, C. M. B. Cordeiro, J. C. Knight, and F. G. Omenetto, "Over 4000 nm bandwidth of mid-IR supercontinuum generation in sub-centimeter segments of highly nonlinear tellurite PCFs," Opt. Express **16**, 7161–7168 (2008).
14. A. F. Fercher, W. Drexler, C. K. Hitzenberger, and T. Lasser, "Optical coherence tomography - principles and applications," Rep. Prog. Phys. **66**, 239–303 (2003).
15. B. Schenkel, R. Paschotta, and U. Keller, "Pulse compression with supercontinuum generation in microstructure fibers," J. Opt. Soc. Am. B **22**, 687–693 (2005).
16. R. Holzwarth, T. Udem, T. W. Hansch, J. C. Knight, W. J. Wadsworth, and P. S. J. Russell, "Optical frequency synthesizer for precision spectroscopy," Phys. Rev. Lett. **85**, 2264–2267 (2000).
17. K. R. Vogel, S. A. Diddams, C. W. Oates, E. A. Curtis, R. J. Rafac, W. M. Itano, J. C. Bergquist, R. W. Fox, W. D. Lee, J. S. Wells, and L. Hollberg, "Direct comparison of two cold-atom-based optical frequency standards by using a femtosecond-laser comb," Opt. Lett. **26**, 102–104 (2001).
18. B. Washburn and N. Newbury, "Phase, timing, and amplitude noise on supercontinua generated in microstructure fiber," Opt. Express **12**, 2166–2175 (2004).
19. B. Washburn, R. Fox, N. Newbury, J. Nicholson, K. Feder, P. Westbrook, and C. Jørgensen, "Fiber-laser-based frequency comb with a tunable repetition rate," Opt. Express **12**, 4999–5004 (2004).
20. C. Gross, T. Best, D. van Oosten, and I. Bloch, "Coherent and incoherent spectral broadening in a photonic crystal fiber," Opt. Lett. **32**, 1767–1769 (2007).
21. J. Nicholson, M. Yan, A. Yablon, P. Wisk, J. Fleming, F. DiMarcello, and E. Monberg, "A high coherence supercontinuum source at 1550 nm," In *Optical Fiber Communications Conference 2003*, Vol. 86 of OSA Proceedings Series (Optical Society of America, Washington, D.C., 2003), pp. 511–512.
22. N. Nishizawa and J. Takayanagi, "Octave spanning high-quality supercontinuum generation in all-fiber system," J. Opt. Soc. Am. B **24**, 1786–1792 (2007).
23. G. Agrawal, *Nonlinear Fiber Optics* (Academic Press, 2001), 3rd ed.
24. J. M. Dudley, G. Genty, and S. Coen, "Supercontinuum generation in photonic crystal fiber," Rev. Mod. Phys. **78**, 1135–1184 (2006).
25. J. Y. Y. Leong, P. Petropoulos, J. H. V. Price, H. Ebendorff-Heidepriem, S. Asimakis, R. C. Moore, K. E. Frampton, V. Finazzi, X. Feng, T. M. Monro, and D. J. Richardson, "High-nonlinearity dispersion-shifted lead-silicate holey fibers for efficient 1-mu m pumped supercontinuum generation," J. Lightwave Technol. **24**, 183–190 (2006).
26. J. J. Miret, E. Silvestre, and P. Andrés, "Octave-spanning ultraflat supercontinuum with soft-glass photonic crystal fibers," Opt. Express **17**, 9197–9203 (2009).
27. Z. Zhu and T. Brown, "Effect of frequency chirping on supercontinuum generation in photonic crystal fibers," Opt. Express **12**, 689–694 (2004).
28. D. Lorenc, D. Velic, A. N. Markevitch, and R. J. Levis, "Adaptive ferntosecond pulse shaping to control supercontinuum generation in a microstructure fiber," Opt. Commum. **276**, 288–292 (2007).
29. J. C. Travers, S. V. Popov, and J. R. Taylor, "Extended blue supercontinuum generation in cascaded holey fibers," Opt. Lett., **30**, 3132–3134 (2005).
30. A. Ferrando, E. Silvestre, P. Andres, J. Miret, and M. Andres, "Designing the properties of dispersion-flattened photonic crystal fibers," Opt. Express **9** 687–697 (2001).
31. E. Silvestre, T. Pinheiro-Ortega, P. Andrés, J. J. Miret, and A. Ortigosa-Blanch, "Analytical evaluation of chromatic dispersion in photonic crystal fibers," Opt. Lett. **30**, 453–455 (2005).
32. E. Silvestre, T. Pinheiro-Ortega, P. Andrés, J. J. Miret, and Ángela Coves, "Differential toolbox to shape dispersion behavior in photonic crystal fibers," Opt. Lett. **31**, 1190–1192 (2006).
33. L. DAVIS, *Handbook Of Genetic Algorithms* (Thomson Publishing Group, 1991), 1st ed.
34. E. Kerrinckx, L. Bigot, M. Douay, and Y. Quiquempois, "Photonic crystal fiber design by means of a genetic algorithm," Opt. Express **12**, 1990–1995 (2004).
35. S. Afshar V. and T. M. Monro, "A full vectorial model for pulse propagation in emerging waveguides with subwavelength structures part I: Kerr nonlinearity," Opt. Express **17**, 2298–2318 (2009).
36. M. D. Turner, T. M. Monro, and S. A. V., "A full vectorial model for pulse propagation in emerging waveguides with subwavelength structures part II: stimulated raman scattering," Opt. Express **17**, 11565–11581 (2009).
37. M. D. O'Donnell, K. Richardson, R. Stolen, A. B. Seddon, D. Furniss, V. K. Tikhomirov, C. Rivero, M. Ramme,

R. Stegeman, G. Stegeman, M. Couzi, and T. Cardinal, "Tellurite and fluorotellurite glasses for fiberoptic raman amplifiers: Glass characterization, optical properties, raman gain, preliminary fiberization, and fiber characterization," J. Am. Ceram. Soc. **90**, 1448–1457 (2007).
38. K. S. Kim, R. H. Stolen, W. A. Reed, and K. W. Quoi, "Measurement of the nonlinear index of silica-core and dispersion-shifted fibers," Opt. Lett. **19**, 257–259 (1994).
39. J. M. Dudley and S. Coen, "Coherence properties of supercontinuum spectra generated in photonic crystal and tapered optical fibers," Opt. Lett. **27**, 1180–1182 (2002).
40. J. Dudley and S. Coen, "Numerical simulations and coherence properties of supercontinuum generation in photonic crystal and tapered optical fibers," IEEE J. Sel. Topics Quantum Electron. **8**, 651–659 (2002).
41. R. R. Alfano, *The Supercontinuum Laser Source: Fundamentals with Updated References* (Springer, 2005), 2nd ed.
42. D. R. Solli, C. Ropers, P. Koonath, and B. Jalali, "Optical rogue waves," Nature **450**, 1054–1057 (2007).
43. R. H. Stolen, J. P. Gordon, W. J. Tomlinson, and H. A. Haus, "Raman response function of silica-core fibers," J. Opt. Soc. Am. B **6**, 1159–1166 (1989).

## 1. Introduction

Supercontinuum (SC) generation is a process of spectral broadening of short pulses that occurs as a result of a cascade of nonlinear processes. It has been studied intensively since it was first discovered [1, 2]. It has a wide range of applications in optical metrology and optical imaging because of its large bandwidth and high intensity [3, 4, 5, 6, 7, 8]. Most of the studies of SC generation performed to date have been based on silica fibers. Due to the properties of silica glass, SC generation has been limited to visible and near infrared wavelengths. Today, with the development of soft glass microstructured optical fibers [9], the effective nonlinear coefficient of fibers can be enhanced by a few orders of magnitudes [10], the group velocity dispersion of the fiber can be tailored to a variety of profiles [9] and the range of operating wavelength can also be extended into mid-infrared [11, 12]. The use of such fibers promises SC applications in the mid-IR such as mid-IR Light Detection and Ranging (LIDAR) [3], mid-IR optical coherence tomography (OCT) [4], mid-IR absorption spectroscopy [5] and mid-IR coherent anti-Stokes Raman scattering (CARS) [6, 7, 8], etc. A Mid-IR SC source would also be a good substitute for current mid-IR sources such as optical parametric oscillators and quantum cascade lasers. Some studies on soft-glass fiber based mid-IR SC generation have demonstrated that they can generate SC up to $4\sim5\mu$m [11, 12, 13]. However, to the best of our knowledge, these mid-IR SC studies have been more focused on generating bandwidth extending into the mid-IR rather than the coherence of the generated SC.

Coherence is a measure of the correlation properties between two pulses. Many SC applications depend upon the coherence such as OCT [14], ultra short pulse compression [15], optical frequency combs for frequency metrology [16, 17, 18, 19, 20], etc. Although the level of coherence (high or low) and the types of coherence (spatial, temporal or spectral) vary from one application to another, the ability to control coherence through fiber design is usually appreciated. The complexity of SC itself makes this control difficult to achieve desired coherence properties by simply scanning the range of potential fiber structures and pump regimes. There are a few cases that allow us to obtain high coherence SC generation [21, 22]. However, these cases are either complicated or do not consider optimizing other aspects of SCG such as bandwidth. Usually, to obtain high coherence, it can be necessary to trade off bandwidth since the main broadening mechanism needs to rely on self-phase modulation. However, achieving required level of coherence and a certain bandwidth over a specified propagation length is not straightforward using the approaches described to date.

The process of SC generation involves multiple physical effects including self-phase modulation (SPM), cross-phase modulation (XPM), four-wave mixing (FWM), stimulated Raman scattering (SRS), soliton fission and dispersive wave generation. [23, 24]. To manipulate the process or the output of a SC requires controls of multiple parameters. This makes it difficult

to find the most optimized set of parameters for specified characteristics. A number of methods have been used in previous studies to tailor the SC spectrum, such as shifting the zero dispersion wavelength (ZDW) [25], flattening dispersion slope [26], tuning pulse chirp [27], modification of the pulse shape [28] and connecting multiple piece of fibers with different dispersion [29]. All of these methods influence the generated SC. However, because of the lack of degrees of freedom (free parameters), their usefulness in the design of SC generation is usually limited, and in general, large parameter space searches are required. For example, shifting the ZDW with respect to the pump wavelength can vary the SC output dramatically. However by doing this, higher order dispersion and nonlinearity also change, which also influences the generated SC. A more advanced example is shown in Ref.[26]. Although this example demonstrates a high level of dispersion control, it first relies on an assumption that the total fiber dispersion is the linear summation of material dispersion and waveguide dispersion ($D_{total} \approx D_{material} + D_{waveguide}$) [30, 31, 32], which is not always appropriate, and second it does not optimize the fiber nonlinearity for SC generation. To extend our ability to control and specify the properties of the generated SC, a more general method is required so that all relevant attributes of a fiber can be considered in SC optimization.

To avoid the need for exhaustive parameter searches, and to increase efficiency, we have developed a Genetic Algorithms (GA) [33] based method to optimize the design parameters of optical fibers. GAs simulate natural selection. They evolve a group of parameters by crossover and mutating the contents of these parameters and mating them according to certain design rules. By doing so, the outputs calculated based on these input parameters can have better overall properties with the increase of generations (iterations) [33]. GAs have been used widely for optimizing complex problems including fiber design for special dispersion profiles [34]. However, to the best of our knowledge, they have never been used to design fiber structures for the purpose of optimizing the bandwidth and coherence of SC generation. In this paper, we demonstrate, for the first time, the use of a GA to design a fiber structure for SC generation and target at large bandwidth and high coherence in mid-IR spectrum.

While GAs are relatively mature algorithms, there is still one major obstacle that needs to be overcome to apply them to this specific problem. Conventionally, GAs work by evaluating a fitness function (in our case a fitness function is related to the SC bandwidth and coherence) based on a set of parameters (in our case the fiber design parameters). In this work, the evaluation of the fitness function starts with a calculation of the fiber nonlinearity and dispersion corresponding to a given fiber design using a finite element method and then the SC bandwidth and coherence using a pulse propagation method (labeled as the "Full Genetic Algorithm Approach" (dashed blue arrows) in Figure 1). However, this full GA approach would be impractical due to the time-consuming pulse propagation. As an example, assuming 1000 structures (i.e., parameter sets, normally called population in GAs [33]) are used and 10 iterations are needed to get the required result then it will take about 11.4 years (10 hours for each structure) to accomplish the job on a typical current computer (2.66 GHz Intel Quad-Core CPU, 4GB 800MHz Memory).

To overcome this obstacle, we develop here a versatile intermediate approach (known here as the Hybrid Approach) to exclude the beam propagation part out of the GA loop. As the red solid arrows shown in Fig. 1, instead of using the full GA approach, we solve this problem with a two-step approach and only use GA for half of it. With this approach, we first explore the relations between fiber properties (dispersion and nonlinearity) and SC output (bandwidth and coherence) through a simplified model and then use a GA to optimize the fiber design based on these relations.

This paper consists of four parts. In Section 2, we discuss the fundamental elements of the pulse propagation method. In Section 3 we explain our simplified model and determine the

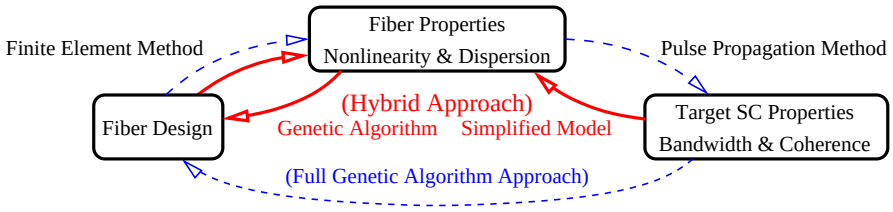


Fig. 1: Schematics of full and hybrid GA approach. Dashed blue arrows form the full GA loop, solid red lines form the hybrid GA loop.

conditions for obtaining large SC bandwidth and high coherence. In Section 4, we start with an initial fiber design and use GA to optimize its structure for the conditions identified in Section 3. Finally, in Section 5 we present the SC output of the optimized fiber design and discuss the results.

## 2. Basics of beam propagation modeling

Before we show the simplified model, a few key components of pulse propagation modeling need to be discussed. Modeling of beam propagation is based on the nonlinear Schrödinger equation (NLSE) which can be written as [23]

$$\frac{\partial A(z,t)}{\partial z}+\frac{\alpha}{2}A(z,t)-\sum_{k\geqslant 2}\frac{i^{k+1}}{k!}\beta_k\frac{\partial^k A(z,t)}{\partial T^k}= i\gamma(1+i\tau_{shock}\frac{\partial}{\partial T})\left(A(z,t)\int_{-\infty}^{\infty}R(T')\times\left|A(z,T-T')\right|^2dT'\right) \quad (1)$$

where A(z,t) is the envelope of the electric field of a propagating pulse $E(x,y,z,t)=A(z,t)F(x,y)e^{i\beta(\omega)z}$. We assume the mode field distribution $F(x,y)$ of different modes do not change during propagation. The propagation constant of the pulse modes $\beta(\omega)$ for specific geometry can be pre-calculated through finite element method (FEM). Here, the coefficients $\beta_k=\partial^k\beta(\omega)/\partial\omega^k|_{\omega=\omega_0}$ are the coefficients in the Taylor series expansion of $\beta(\omega)$ around frequency of input pulse $\omega_0$. $\alpha$ represents the loss calculated based on the material and confinement loss and $\gamma$ is the effective nonlinear coefficient of the fiber. Details of the definitions of these parameters are shown in Appendix I (Eq. (6-9)). It should be noted that Eq. (1) is derived in the regime where the weak guidance approximation is valid. A full vectorial pulse propagation model [35, 36] should be used in order to accurately describe the nonlinear and dispersive effects in fibers with high index glasses and sub-wavelength structures. However, the hybrid GA method proposed here could still be applied to the full vectorial model, which is beyond the scope of this paper.

The Schrödinger equation Eq. (1) is solved numerically using a split-step-Fourier method. As part of this procedure, the dispersion terms $\sum_{k\geqslant 2}(i^{k+1}/k!)[\beta_k\partial^k A(z,t)/\partial T^k]$ are included in the frequency domain using $\beta(\omega)\tilde{A}(\omega)$ where $\tilde{A}(\omega)$ is the Fourier transform of A(t) [23]. The frequency dependence of $\gamma$ is calculated through optical shock term $\tau_{shock}$. The modeling work presented here is based on a type of Tellurite glass ($70TeO_2-10Na_2O-20ZnF_2$) [37]. Its Raman response function and Raman fraction are calculated using Eqs. (14) and (15) (see details in Appendix I) and the Raman gain spectrum as shown in Fig. 2.

The Raman fraction $f_R$ is equal to 0.064 for this composition of glass (see the derivation in Section 7, Eq. (10-15)). Although this value is about 3 times smaller than that of silica glass (0.18), the fact that the nonlinear refractive index $n_2$ of this tellurite glass ($5.9\times10^{-19}m^2/W$) is

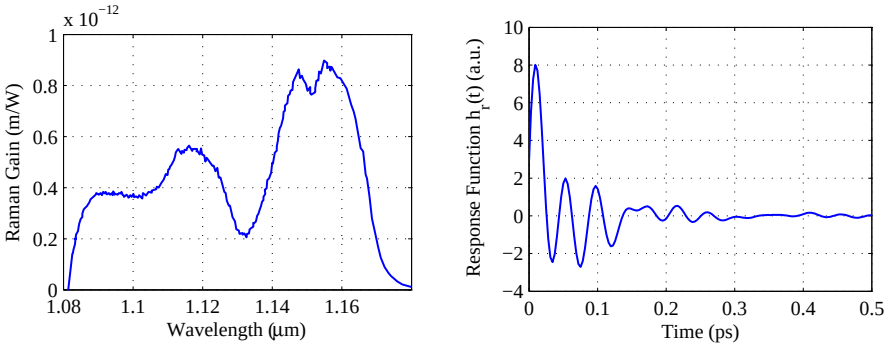


Fig. 2: Raman gain spectrum of $70TeO_2 - 10Na_2O - 20ZnF_2$ glass, pumped at 1060nm [37] (left) and calculated Raman response function using the maximum Raman gain at 1155nm (right)

much higher than silica glass ($2.36 \times 10^{-20} m^2/W$) [38] results in much higher Raman response ($\gamma f_R h_R(t)$ see Appendix I) for tellurite glass than silica glass.

In this paper, the spectrum coherence of a SC output refers to mutual pulse coherence and it is defined as Eq. (2) [39];

$$\left|g_{12}^{(1)}(\lambda, t_1 - t_2)\right| = \left| \frac{\langle E_1^*(\lambda, t_1) E_2(\lambda, t_2) \rangle}{\sqrt{< |E_1(\lambda, t_1)|^2 >< |E_2(\lambda, t_2)|^2 >}} \right|, \tag{2}$$

where $E_1$ and $E_2$ are the electric fields of two pulses from two different shots, $\lambda$ is wavelength, $t_1$ and $t_2$ are time. To calculate coherence, shot noise is randomly introduced into each initial pulse and 20 such pulses are taken for each coherence calculation [40]. For convenience, we also use average coherence $< |g_{12}^{(1)}| >= \int |g_{12}^{(1)}(\lambda, 0)||E(\lambda)|^2 d\lambda / \int |E(\lambda)|^2 d\lambda$ to describe the overall coherence of a pulse across the spectrum [24]. The bandwidth of the generated SC is defined as the width at 20dB of the maximum point in the spectrum.

## 3. Simplified models

The main nonlinear effects that are involved in SC generation include SPM, XPM, FWM, SRS, soliton fission and dispersive wave generation [24, 41]. Depending on the fiber properties (nonlinearity and dispersion) and inputs conditions (pulse width, intensity, wavelength, chirp, etc.), the detailed mechanisms underpinning SC generation can vary dramatically [24]. This indicates an important difference between SC generation and individual linear-nonlinear effects like SPM, XPM, FWM, SRS, etc. While for the individual processes there is usually an approximate analytical relation that can be used to find the optimized conditions of the process, for SC generation, we have to rely on numerical methods. Furthermore, although SC generation can always be predicted numerically when all required initial conditions are provided, noise can be a critical aspect for the SC process because of the modulation instability (MI). In particular, "Rogue waves" [42] in optical fiber (optical solitons) can make the outputs of SC generation so different from pulse to pulse that only statistical predictions can be made.

Although the broadening process has random factors, we still can build up a basic understanding of the relations among fiber nonlinearity, dispersion, SC bandwidth and coherence by exploring different combinations of nonlinearity and dispersion profiles. However, the infinite possible combinations still make this exploration process too complicated to be useful. That is

why simplified models are required to explore the physics of combined linear and nonlinear processes involved in SC generation.

The simplified model will be used as guide line for defining the fitness function for the GA. While this choice is not unique and influences the accuracy of predicting the output SC in the final fiber. Because of this, it may require a few iterations before an appropriate simplified model can be decided for practical use. For purpose of this paper, to show the feasibility of using a hybrid GA to effectively design fibers to generate SC with particular desired characteristics. We approximate dispersion and nonlinearity to the first order (i.e. we use constant dispersion and nonlinearity). Together with Raman response function, we use the simplified model to explore the relationship between the nonlinearity and dispersion of fibers and the bandwidth and coherence of SC outputs. In this simplified model, the UV cutoff and IR cutoff are set at 0.4$\mu$m and 6$\mu$m respectively. The loss around the cutoffs is interpolated with exponential functions and the loss between these cutoffs is assumed to be zero.

Figures 3 and 4 show the bandwidth and coherence variation of the SC generation of a 100 fs, 10 kW peak power pulse propagating along the fiber from 0 to 50 mm for values of D = -5 to 5 (ps/nm/km) and $\gamma$ = 100 and 200 ($W^{-1}km^{-1}$). The basic trends of the spectral broadening and coherence degradation as shown in the figures can be summarized as follows: 1) the coherence decreases as either nonlinearity or dispersion increases, and it mainly happens in anomalous dispersion regime, 2) the bandwidth increases as either nonlinearity or dispersion increases and it increases dramatically in anomalous dispersion regime. By analyzing the spectrum evolution of the propagating pulse, it is clear that: 1) in the normal dispersion region, SPM dominates the broadening, (2) in the anomalous dispersion region, FWM, MI and soliton fission dominate the broadening.

It can be inferred from the results shown here that a broad bandwidth SC that is only limited by transmission window of that fiber can readily be obtained from SC generation based on fibers with anomalous dispersion and large nonlinearity. However, the coherence reduces dramatically in this regime. On the other hand, although the spectral broadening is relatively slow in the normal dispersion regime, a broad bandwidth can still be obtained with large nonlinearity and small absolute values of dispersion (for comparatively long propagation lengths). Furthermore, no obvious coherence degradation is observed for small absolute values of dispersion. Therefore, for the purpose of designing a large bandwidth and highly coherent SC source, fibers with high nonlinearity and flat small absolute values of dispersion are preferred. It is worth mentioning that the conclusions obtained here are based on some simplifications. In reality, both nonlinearity and dispersion are wavelength dependent, and thus the broadening of pulses differs from the simplified models. However, this simplified model provides important information (at least to first order) about the relation between SC bandwidth and coherence and fiber nonlinearity and dispersion, which is used in the next section for the GA to generate fiber structures that are suitable for this purpose.

## 4. Fiber structure design and genetic algorithms

Based on the results of the simplified model shown above, we seek to use a Genetic Algorithm to design a fiber [33]. When using a GA, the choice of initial fiber structure is as important as the definition of an appropriate "fitness function", which quantifies the suitability of the properties of the fiber for the purpose of generating coherent broadband SC. The initial fiber structure needs to contain several free parameters that control the structure, and ideally, its topology should be capable of supporting a broad range of variations in the fiber properties (particularly nonlinearity and dispersion). From previous reports, we know that structures with small cores are able to provide high nonlinearity [25, 10] and structures with relatively more glass in the cladding (such as rings-of-holes structures) can in some cases provide flat and low disper-

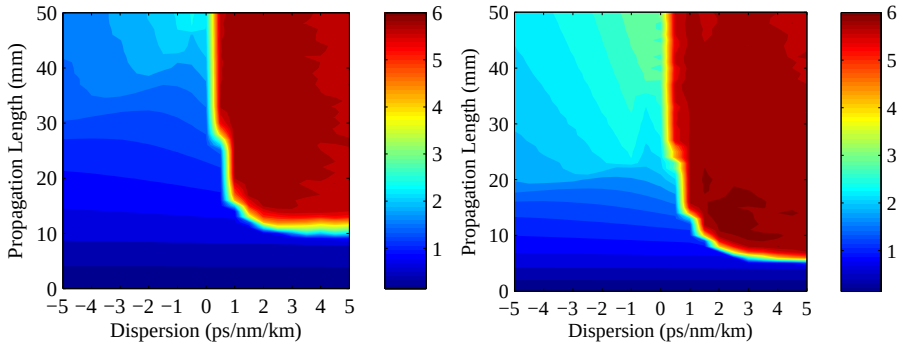


Fig. 3: 20dB Bandwidth, in $\mu m$, of generated SC output with different constant dispersion D and nonlinearity $\gamma$ at different propagation length.

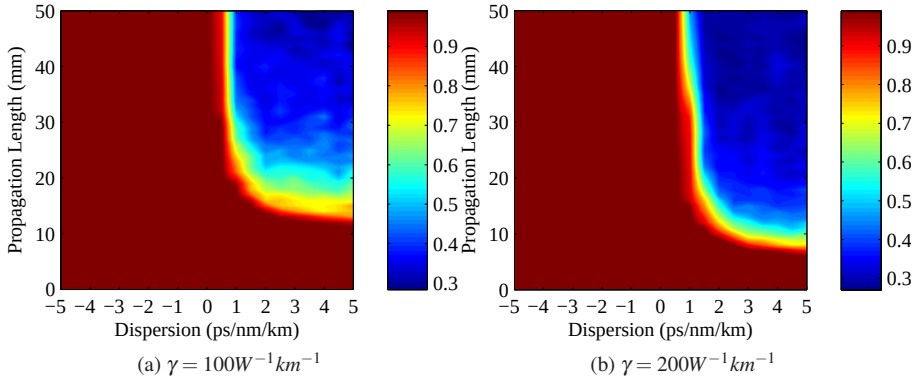


Fig. 4: Coherence $< |g_{12}^{(1)}| >$ of the outputs of SC generation with different constant dispersion and nonlinearity at different propagation length. $< |g_{12}^{(1)}| >$ = 1 is maximum value associated with perfect coherence

sion [34]. The design of the initial structure also takes account two other aspects: confinement loss and fabrication distortion. To reduce confinement loss and minimized glass flow between core and cladding regions during fiber drawing, we decided to use a double cladding structure with inner structure providing special optical properties and suspended by the outer structure through thin struts to provide high confinement.

Based on this knowledge, an initial fiber geometry is designed based on the geometry shown in Fig. 5. This geometry is defined by a set of parameters R1, R2, R3, R4, R5, r1, r2, r3, L1 and L2. Depending on the values chosen for these parameters, this structure can vary from a small-core structure with high nonlinearity (when core region (R3) is small) to rings-of-holes structure (when inner six holes are at similar size and sit at middle of the core region). In order to increase the efficiency of this GA calculation, only R1, R3, R4, r1, r2 and L1 are set as free parameters.

In a GA, the fitness function acts as a figure of merit and its value can quantitatively describe the goodness or badness of the input information (structure parameters). In order to choose

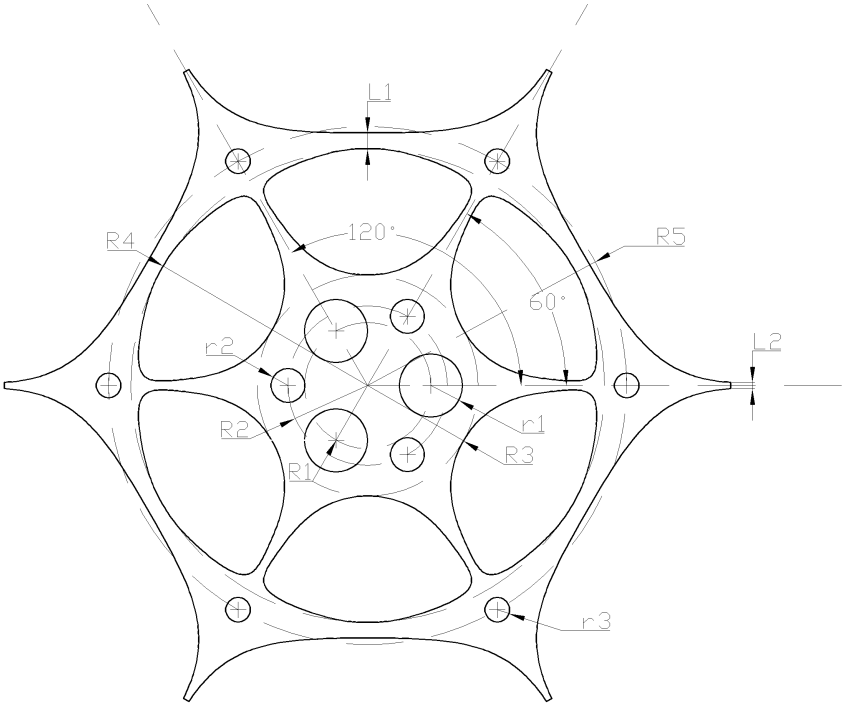


Fig. 5: Initial design of the fiber structure.

an appropriate expression of fitness for this problem, we have to take account of fiber nonlinearity and dispersion, where the dispersion includes material (via the Sellmeier equation) and waveguide dispersion effects.

The material dispersion always exhibits large negative values at short wavelengths and large positive values at long wavelengths. The waveguide dispersion cannot cancel the material dispersion in those regimes unless the fiber structure is operating in the extreme sub-wavelength regime (when the core size is much smaller than wavelength). In such cases, both material and waveguide dispersion are insensitive to the fiber structure. For fibers with relatively large core diameter, the cutoff wavelength of glass transmission is usually reached before the dispersion at that wavelength becomes insensitive to the structure. Therefore, in the dispersion profile of a non-sub wavelength fiber, there still are large negative and large positive values at short and long wavelengths respectively. Only in the middle region, where waveguide dispersion values can have similar magnitude of material dispersion, that the total dispersion can be effectively manipulated via the choice of the fibre structure. Based on this information, we choose to define the fitness function as:

$$F = \gamma_{pump} \times (\sum_i |D_i|)^{-1} \tag{3}$$

where $\gamma_{pump}$ is the nonlinearity at pump wavelength and $D_i$ are the dispersion values across the wavelength region for which we strive for flat dispersion. The reason for taking the summation in Eq. (3) instead of integrating is to reduce the number of points used in the calculation to speed up the modeling. This fitness function is consistent with the results of our simplified model in Sec. 3 that large nonlinearity and small absolute values of dispersion are required

for large bandwidth highly coherent SC generation, since both large nonlinearity and small dispersion will result in large fitness. This is not the only definition for the fitness function that could be used. Other choices can also be used as long as the fiber structures converge as the fitness increases (or decreases). For simplicity and to make the numerical calculation viable, we only use three dispersion values at wavelengths $\lambda$ = 2000 nm, 2500 nm and 3000 nm for the summation on the denominator of Eq. (3).

In our GA model, we use 1000 parameter sets (each set consists of values for R1, R3, R4, r1, r2 and L1). The crossover functions are defined as Eq. (4) and (5), which are used in the mating process of GAs to create new generation without losing old genetic information. See details in Ref.[33].

$$Pset_{new}^{(1)} = \alpha \times Pset_{old}^{(1)} + (1-\alpha) \times Pset_{old}^{(2)} \tag{4}$$

$$Pset_{new}^{(2)} = (1-\alpha) \times Pset_{old}^{(1)} + \alpha \times Pset_{old}^{(2)} \tag{5}$$

Where $Pset_{new}^{(*)}$ are new generated parameter sets, $Pset_{old}^{(*)}$ are old parameter sets and $\alpha$ is a random number between 0 and 1. The mutation rate (see Ref. [33]) is set to 20% which is found to be a good ratio for this model. After 6 iterations, the output of this GA model is the structure in Fig. 6(a) whose dispersion shows a low flat region between $2 \sim 3$ ($\mu$m) as shown in Fig. 6(b). The variation of dispersion is about $\pm 2$ ps/km/nm within this wavelength range where nonlinearity is in the range of $68 \sim 174$ ($W^{-1}km^{-1}$). It is worth mentioning that this range of nonlinearities are far smaller than the maximum nonlinearity that can be achieved in this glass (calculated around 1500 $W^{-1}km^{-1}$ with R3 close to 0.65 $\mu$m). In addition, the nonlinearity decreases quickly with increasing of wavelength as it is evident in Fig. 6. This is because of the effective mode area increases quickly with wavelength, and the spatial location of the guided mode transitions from being confined within the central six holes, to seeing the scalloped hexagonal as the core. This result shows the efficiency of GA (since only 6 iterations were taken) for this problem. It also demonstrates the capability for achieving dramatic dispersion control with our new fiber design.

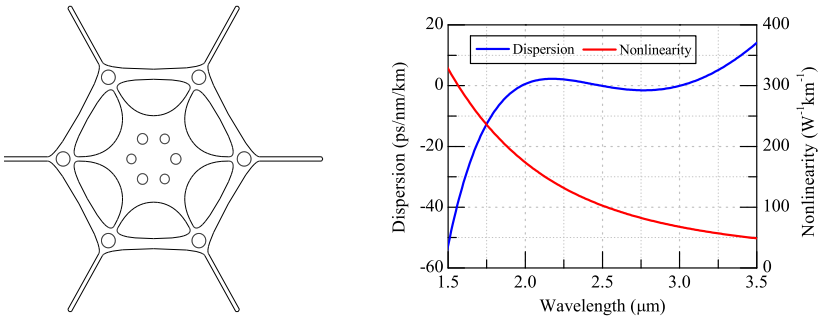


Fig. 6: Optimized structure (a) and its corresponding dispersion and nonlinearity (b).

The stability of the convergence of the GA for this problem was investigated through study of a subset of GA outputs with fitness values larger than 100 nm/ps/W within the last generation (iteration). Their nonlinearity and dispersion profiles are shown in Fig. 7. Within this subset, the maximum difference in dispersion among these samples is about 5ps/nm/km and the maximum difference in nonlinearity at 2 $\mu$m is about 40 $W^{-1}km^{-1}$. The variation of each parameter of

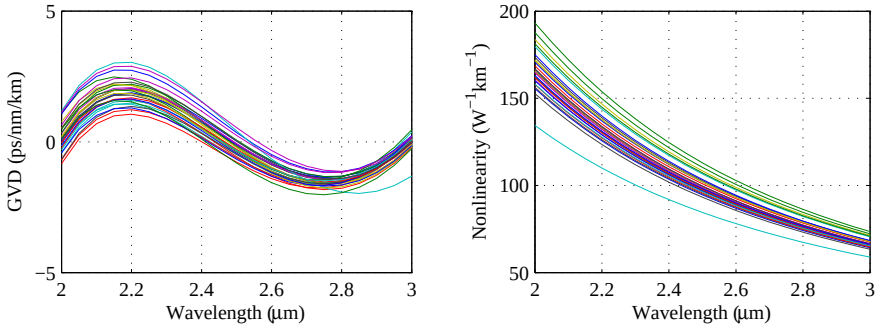


Fig. 7: Dispersion(left) and nonlinearity(right) of a range of samples.

the structure are listed in Table 1. The last column of Table 1 shows the relative change of each structural parameter within the subset, which indicates the potential influences of each parameter brought in by fabrication.

Table 1: Statistics of the structure parameters

| | Average ($\mu m$) | Standard Deviation ($\mu m$) | Relative Error |
|---|---|---|---|
| R1 | 1.64e-006 | 8.03e-009 | 0.49% |
| r1 | 4.05e-007 | 1.01e-008 | 2.49% |
| r2 | 3.16e-007 | 8.14e-009 | 2.57% |
| R3 | 3.20e-006 | 8.50e-009 | 0.26% |
| R4 | 6.24e-006 | 6.54e-007 | 10.48% |
| L1 | 1.17e-006 | 1.76e-007 | 15.02% |

From this table, it is clear that the position of the six holes in the center region (R1) and the amount of glass around these holes (R3) are particularly critical. The size of the center six holes are also important parameters. The standard deviations of r1 and r2 are smaller than the difference between them, which means r1 and r2 need to be different in order to have fine control of dispersion and there are at least two localized solutions around the average radius of these two since the symmetry of the fiber geometry shows they are exchangeable. The influence of the outer ring (R4) and its thickness (L1) is clearly less. These results tell us that, in fabrication, more attention needs to be paid to the central structure rather than outer parts, which is unsurprising.

## 5. SC generation in optimized structure and discussion

As discussed in Section 4, unlike the ideal constant dispersion cases, any practical fibers always have large negative (normal) and positive (anomalous) dispersion for short and long wavelengths respectively. The fiber nonlinearity is also wavelength dependent. Nonlinearity decreases as wavelength increases as result of nonlinear refractive index decreases and effective mode area increases. These wavelength dependencies make the choice of pumping wavelength critical for SC generation (in practice, one should choose the pumping wavelength before designing and optimizing the fiber). To investigate this in detail, in the following, we use the optimized fiber structure developed in the previous section and predict the generated SC when

it is pumped with pulses that have 10 kW peak power and 100 fs width at wavelengths ranging from 1500 nm to 3500nm.

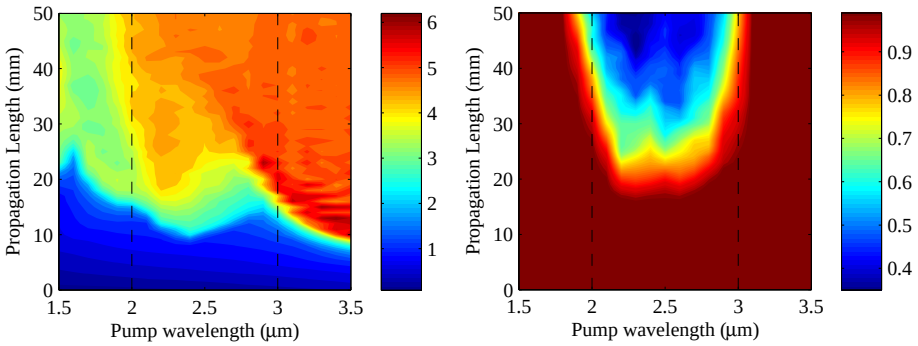


Fig. 8: Bandwidth (left) and coherence (right) of SC outputs with different pump wavelengths in the optimized fiber. Between the vertical dashed lines is the region of optimization.

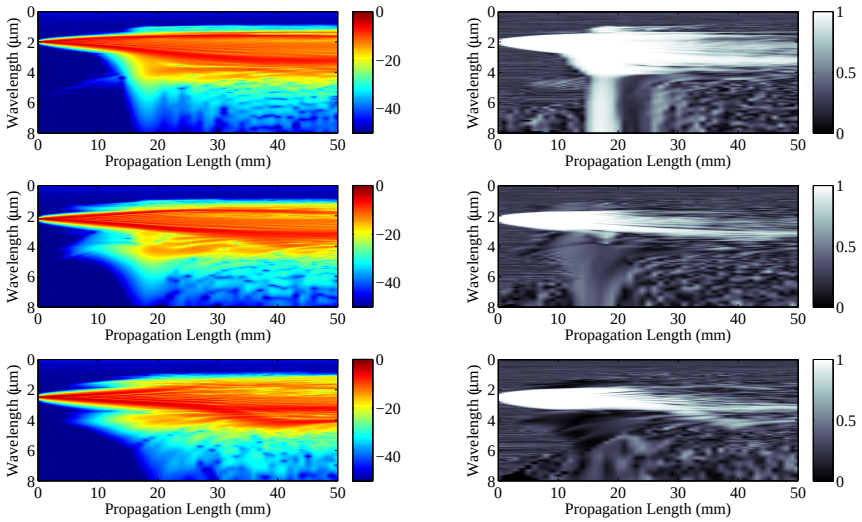


Fig. 9: Normalized intensity (left) and coherence (right) spectrums of pulses propagating along the optimized fiber pump at 2, 2.2, 2.5 $\mu m$ from top to bottom respectively.

Figure 8 shows the bandwidth and coherence of the pulses propagating along the fiber. Recall that the fiber design developed in previous section is optimized for SC generation in the spectrum region of $2 \sim 3\mu m$ (region between the dashed lines). In this region, as indicated in Fig. 8, the bandwidth initially increases as pump wavelength increases. However, this is then followed by a decrease and an increase as the pump wavelength increases towards the end of the spectrum ($\sim 3\mu m$). On the contrary, the coherence first decreases and then increases as the pump wavelength increases. According to the results of the simplified model, large values of nonlinearity or dispersion result in large bandwidth and low coherence, small values of nonlinearity or dispersion result in small bandwidth and high coherence. The changes in the bandwidth and coherence in Fig. 8 are due to the increase of the average dispersion and decrease of average nonlinearity across the pulse spectrum. For a certain propagation length, e.g. 20 mm, the pulse

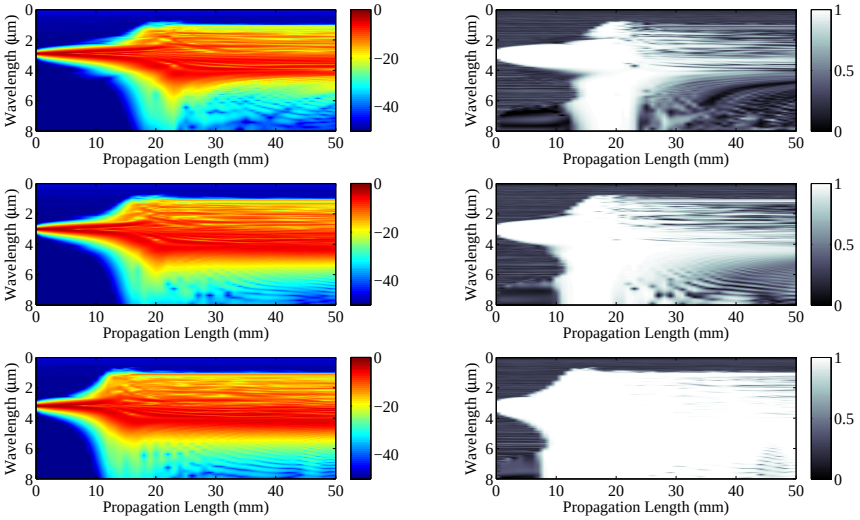


Fig. 10: Normalized intensity (left) and coherence (right) spectrums of pulses propagating along the optimized fiber pump at 2.9, 3, 3.2 $\mu m$ from top to bottom respectively.

spectrum moves into flat near-zero dispersion region when the pump wavelength moves from 2 to 2.2 $\mu m$, and then moves gradually into anomalous dispersion region when the pump wavelength from 2.2 to 3 $\mu m$. However, during this process, the nonlinearity drops more than a half as the pump wavelength increases from 2 to 3 $\mu m$. This is the reason why the bandwidth decreases for pump wavelengths around $2.5\mu m$ and the coherence increases slightly around the same region. Fig. 9 shows the intensity and coherence spectrums of SC generations pumped at 2, 2.2, and 2.5 $\mu m$, from top to bottom respectively. The decrease of coherence along the propagation for these cases (also shown as the decrease of average coherence in Fig. 8 at corresponding pumping wavelength) is due to the anomalous dispersion after $3\mu m$ of this fiber design (Fig. 6(b)). This is explained in Appendix II. As the pulse sees more anomalous dispersion, MI start to have more impact on the broadening as can be seen in the side bands of the 2.2 and 2.5 $\mu m$ pumped cases in Fig. 9. For pump wavelengths longer than about $2.7\mu m$, the pump is in the anomalous dispersion regime and nonlinearity is low. Once the pulse is broadened initially, there is not enough power to arise sufficient nonlinear effects to cause the decrease of coherence. That is why the generated bandwidth is large but coherence remains high. Corresponding examples are given in Fig. 10, which show the intensity and coherence spectrums of pulses pumped at 2.9, 3, and 3.2 $\mu m$ from top to bottom respectively.

In order to show the enhancements of bandwidth and coherence that can be achieved with our new design (Fig. 6), we compare its spectral output with that of a $10\mu m$ diameter tellurite glass rod surrounded by air which also has zero dispersion around $2\mu m$. The dispersion profile of the rod calculated using the same Sellmeier equation as we used for our new design, is shown in Fig. 11. Fig. 12 and Fig. 13 shows the comparison of the SC bandwidth and coherence of three cases: a) the optimized structure, b) 10 $\mu m$ rod and c) an artificial case of a 10 $\mu m$ rod with the nonlinearity of the optimized structure. Fig. 12 is the evolution of the intensity and coherence spectra of SC generation along the propagation direction. The pump wavelength is 2 $\mu m$. Case b) does not display much spectral broadening although the coherence is high due to relatively low nonlinearity of the rod (47.3 $W^{-1}km^{-1}$ at 2 $\mu m$). Recall the optimization of our design is to achieve high coherence as well as large bandwidth. So case b) is not ideal.

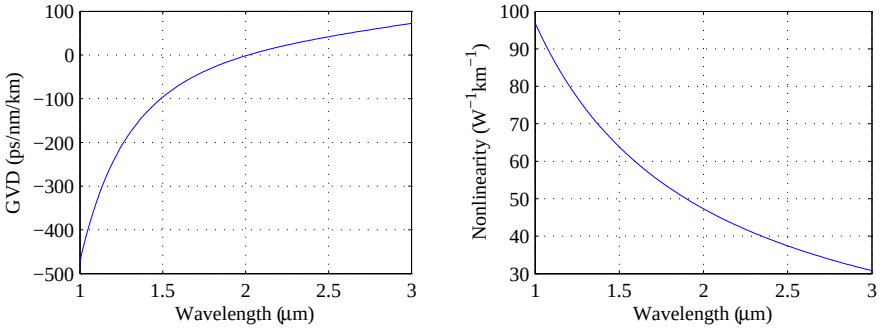


Fig. 11: Dispersion and nonlinearity of a 10$\mu m$ diameter Tellurite rod surrounded by air.

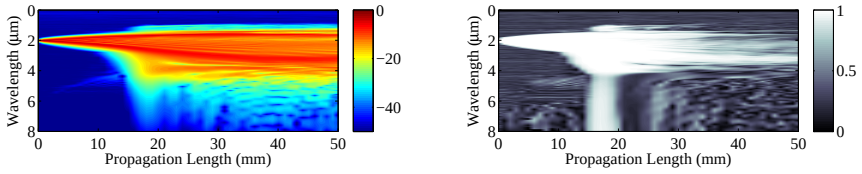


(a) Optimized structure

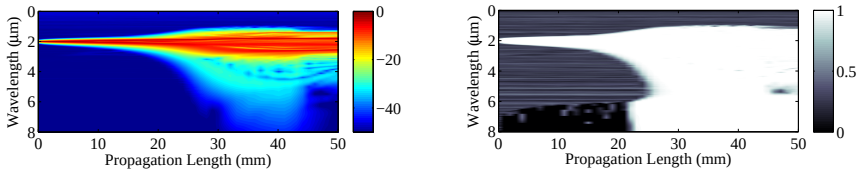


(b) 10 $\mu m$ diameter rod

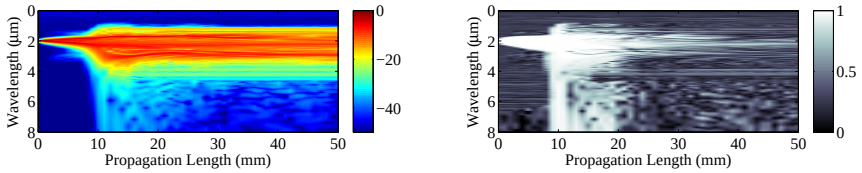


(c) 10 $\mu m$ diameter rod with the nonlinearity profile of optimized structure

Fig. 12: Intensity (left) and coherence (right) spectra of a pulse propagating along the fiber with different dispersions and nonlinearities. a) For dispersion and nonlinearity profiles of optimized structure, shown in Fig. 6, b) for dispersion and nonlinearity profiles of 10 $\mu m$ diameter rod, shown in Fig. 11, c) for dispersion profile of 10 $\mu m$ diameter rod with nonlinearity profile of the optimized structure.

Case c) has larger bandwidth than case b) due to higher nonlinearity. Comparing c) to a), the bandwidth of c) broadens at a shorter propagation length than a) but the final bandwidth of c) is not as large as a) and its coherence is also lower than the one of a). Fig. 13 shows the same conclusion in a different form. These comparisons show that the fiber structure optimized by the hybrid GA approach does have better SC performance in terms of both large bandwidth and high coherence than conventional fiber designs.

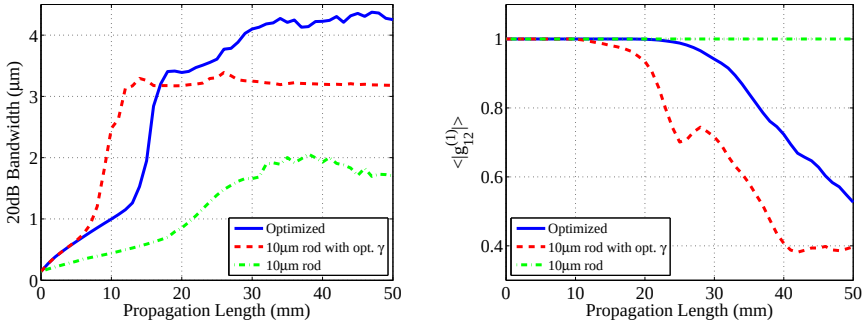


Fig. 13: 20dB bandwidth (left) and coherence (right) of SCG with dispersion and nonlinearity profiles of optimized structure (Fig. 6), 10 $\mu m$ diameter rod (Fig. 11) and 10 $\mu m$ diameter rod with nonlinearity profile of optimized structure.

## 6. Conclusion

In this paper we demonstrated the first application of GAs to design fibers that are optimally suited for SC generation. A hybrid approach is introduced to increase the efficiency and practicality of GAs for SC generation. In our hybrid approach, we considered a simple case of constant nonlinearity and dispersion and found the relation between the coherence and bandwidth of the SC generation as a function of constant nonlinearity and dispersion. This relation was used to establish the fitness function for the GA model. Although, the choice of the initial simplified case is not unique, the one used here provides insight into the regimes that produce coherent SC. It is computationally efficient and leads to fiber designs with high SC coherence and bandwidth.

Applications of this hybrid approach and the prototype of our new fiber design are not limited to design SC generation. Other applications can take advantage of this hybrid approach. For example, it could be used to optimize the gain bandwidth and the phase matching condition of an optical parametric oscillator (OPO). Although there are already known relations for OPO such as relations for gain wavelength and bandwidth, and we can use these relations directly, the hybrid approach still can be useful if other characteristics apart from the gain wavelength and bandwidth needed to be optimized.

## 7. Appendix I: Definition of components in nonlinear Schrödinger Equation

The effective nonlinear coefficient is defined as [23]

$$\gamma = \frac{2\pi}{\lambda_0}\frac{n_{2,eff}}{A_{eff}} \tag{6}$$

where $\lambda_0$ is the wavelength of input pulse, and

$$n_{2,eff} = \frac{(\iint_{-\infty}^{\infty} n_2(x,y)\,|F|^2\,dxdy)^2}{\iint_{-\infty}^{\infty}|F|^4\,dxdy}, \tag{7}$$

$$A_{eff} = \frac{(\iint_{-\infty}^{\infty} |F|^2\,dxdy)^2}{\iint_{-\infty}^{\infty}|F|^4\,dxdy}. \tag{8}$$

$\tau_{shock}$ in Eq. (1) is the optical shock time which is defined as [24]

$$\tau_{shock} = \frac{1}{\omega_0} - \frac{1}{n_{eff}(\omega_0)} \frac{\partial n_{eff}(\omega)}{\partial \omega}|_{\omega_0} - \frac{1}{A_{eff}(\omega_0)} \frac{\partial A_{eff}(\omega)}{\partial \omega}|_{\omega_0} \tag{9}$$

where $n_{eff}$ is the effective refractive index of the propagating modes. $R(t)$ in Eq. (1) is the nonlinear response function which is defined as [23]

$$R(t) = (1 - f_R)\delta(t) + f_R h_R(t) \tag{10}$$

where $f_R$ is the Raman fraction and $h_R(t)$ is Raman response function. The first term represents instantaneous nonlinear effects and the second term represents delayed effects. Previously, in silica glass, $f_R$ is estimated by using the peak value of the Raman gain [23]. However, this is not accurate for glasses with multiple peaks in Raman gain. In this work, the Raman fraction $f_R$ is calculated through an integration over the Raman gain spectrum. According to Ref.[43], the complex nonlinear refractive index can be expressed as

$$N_2(\Omega) = f_R N_2(0) \tilde{h}_R(\Omega) \tag{11}$$

where $\Omega = \omega - \omega_0$, $N_2(0) = n_2(\omega_0)$. The imaginary part of the nonlinear refractive index $N_2(\Omega)$ can be expressed in terms of Raman gain [43],

$$Im(N_2(\Omega)) = \frac{\lambda_0 g(\Omega)}{4\pi} \tag{12}$$

use the Kramers-Kronig relations, we can obtain the real part the $N_2(\Omega)$ and express $N_2(\Omega)$ as

$$N_2(\Omega) = (\frac{\lambda_0}{4\pi} \frac{1}{\pi} \mathscr{P} \int_{-\infty}^{\infty} d\Omega\prime \frac{g(\Omega)}{\Omega\prime - \Omega}) + i(\frac{g(\Omega)\lambda_0}{4\pi}) \tag{13}$$

where $\mathscr{P}$ is Cauchy principle value. Take inverse Fourier transform on Eq. (11) and then integrate over $t$ on both side, and recall $\int_0^{\infty} h_R(t)dt = 1$, therefore we have

$$h_R(t) = \frac{\mathscr{F}^{-1}(N_2(\Omega))}{\int_0^{\infty} \mathscr{F}^{-1}(N_2(\Omega))dt} \tag{14}$$

$$f_R = \frac{\int_0^{\infty} \mathscr{F}^{-1}(N_2(\Omega))dt}{N_2(0)} \tag{15}$$

Notice the symmetry of the real part and the antisymmetry of the imaginary part of $N_2$, the integral been taken in $f_R$ is real.

## 8. Appendix II: Cause of coherence degradation

The degradation of coherence occurs due to the fact that the anomalous dispersion tail that starts to dominate from $3\mu m$ as a result of the increasing role of material dispersion in this regime. To prove this, we compare the coherence from the dispersion profile in Fig. 6 to the ones from a couple of artificial dispersion profiles as shown in Fig. 14. The dispersion profile MOD1 is modified based on profile ORIG where the flattened region is extended from $2 \sim 3\mu m$ to $2 \sim 4\mu m$. The dispersion profile MOD2 is obtained by inverting the tail of ORIG profile from the point when the derivative is zero. The third artificial dispersion profile MOD3 is also obtained by inverting the tail of MOD1 profile. Fig. 14b shows the behavior of coherence as a function of propagation length for all the profiles. The behavior of coherence in MOD1 is similar to ORIG, i.e., it decreases after a certain length of propagation, but the degradation happens at longer lengthes compared to ORIG. In contrast, MOD2 and MOD3 do not show any obvious loss in coherence.

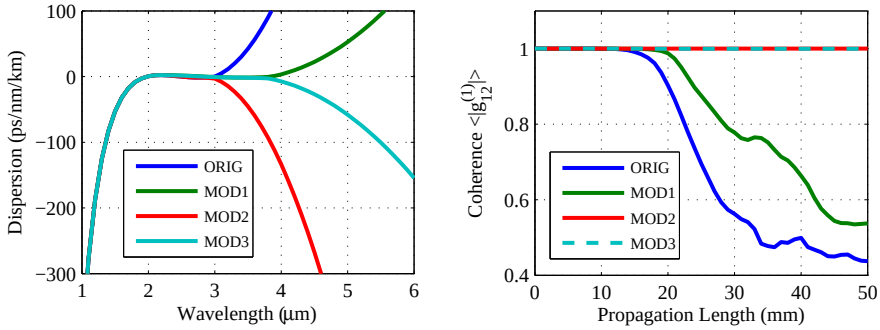


(a) (b)

Fig. 14: Dispersion curves and corresponding coherence of the SC outputs. Curve ORG is the original dispersion curve calculated from GA modeling, MOD1 to MOD3 are the artificial dispersion curves

**Acknowledgments**

Tanya M. Monro acknowledges the support of an ARC Federation Fellowship.